Journal Pre-proof

Quantifying the discrepancies in the geometric and mechanical properties of the theoretically designed and additively manufactured scaffolds

Yongtao Lu, Zhentao Cui, Liangliang Cheng, Jian Li, Zhuoyue Yang, Hanxing Zhu, Chengwei Wu

PII: S1751-6161(20)30629-9

DOI: https://doi.org/10.1016/j.jmbbm.2020.104080

Reference: JMBBM 104080

To appear in: *Journal of the Mechanical Behavior of Biomedical Materials*

Received Date: 12 June 2020

Revised Date: 2 September 2020

Accepted Date: 6 September 2020

Please cite this article as: Lu, Y., Cui, Z., Cheng, L., Li, J., Yang, Z., Zhu, H., Wu, C., Quantifying the discrepancies in the geometric and mechanical properties of the theoretically designed and additively manufactured scaffolds, *Journal of the Mechanical Behavior of Biomedical Materials* (2020), doi: https://doi.org/10.1016/j.jmbbm.2020.104080.

2nd September 2020

Dear the Journal of the Mechanical Behavior of Biomedical Materials,

Please find enclosed the revised manuscript entitled 'Quantifying the discrepancies in the geometric and mechanical properties of the theoretically designed and additively manufactured scaffolds' (manuscript number: JMBBM-D-20-00612R1), which I am submitting for consideration of publication as a research article in the Journal of the Mechanical Behavior of Biomedical Materials.

Here I confirm that all the authors were fully involved in the study, preparation and revision of the manuscript and that the material within is our own original work and has not been and will not be submitted for publication elsewhere. Thanks for your consideration. Please feel free to send all correspondence concerning this manuscript to me by email.

Sincerely,
Yongtao

Yongtao Lu, Ph.D
Department of Engineering Mechanics
Dalian University of Technology
No.2 LingGong Road,Dalian 116024, China
Email: yongtaolu@dlut.edu.cn , yongtolu@hotmail.com

Quantifying the discrepancies in the geometric and mechanical properties of the theoretically designed and additively manufactured scaffolds

Yongtao Lu[1,2,3], Zhentao Cui[1], Liangliang Cheng[4,*], Jian Li[5], Zhuoyue Yang[1], Hanxing Zhu[6] and Chengwei Wu[1,2,*]

[1]Department of Engineering Mechanics, Dalian University of Technology, No. 2 Linggong Road, 116024, Dalian, China
[2]State Key Laboratory of Structural Analysis for Industrial Equipment, Dalian University of Technology, No. 2 Linggong Road, 116024, Dalian, China
[3]DUT-BSU Joint Institute, Dalian University of Technology, Dalian, 116024, China
[4]Department of Orthopedics, Affiliated Zhongshan Hospital of Dalian University, Dalian 116001, China
[5]Beijing Key Laboratory of Rehabilitation Technical Aids for Old-Age and Disability, Key Laboratory of Rehabilitation Aids Technology and System of the Ministry of Civil Affairs, National Research Center for Rehabilitation Technical Aids, Beijing 100176, China
[6]School of Engineering, Cardiff University, Queen's Buildings, the Parade, CF24 3AA, Cardiff, UK

CORRESPONDING AUTHORS:

Chengwei Wu, Ph.D
Department of Engineering Mechanics,
Dalian University of Technology,
No. 2 Linggong Road, Ganjingzi District
116024, Dalian, China
Email: cwwu@dlut.edu.cn

LiangLiang Cheng, M.D.
Department of Orthopaedics,
Affiliated Zhongshan Hospital of Dalian University,
No. 6 Jiefang Street, Zhongshan District, Dalian 116001, China
Email: liangliang30766@163.com

Number of words (Introduction to conclusion): 4950

Number of figures: 9

Number of tables: 0

Abstract

In recent years, the triply periodic minimal surface (TPMS) has emerged as a new method for producing open cell porous scaffolds because of the superior properties, such as the high surface-to-volume ratio, the zero curvature, etc. On the other hand, the additive manufacturing (AM) technique has made feasible the design and development of TPMS scaffolds with complex microstructures. However, neither the discrepancy between the theoretically designed and the additively manufactured TPMS scaffolds nor the underlying mechanisms is clear so far. The aims of the present study were to quantify the discrepancies between the theoretically designed and the AM produced TPMS scaffolds and to reveal the underlying mechanisms, e.g., the effect of building orientation on the discrepancy. 24 Gyroid scaffolds were produced along the height and width directions of the scaffold using the selective laser melting (SLM) technique (i.e., 12 scaffolds produced in each direction). The discrepancies in the geometric and mechanical properties of the TPMS scaffolds were quantified. Regarding the geometric properties, the discrepancies in the porosity, the dimension and the three-dimensional (3D) geometry of the scaffolds were quantified. Regarding the mechanical properties, the discrepancies in the effective compressive modulus and the mechanical environment (strain energy density) of the scaffolds were evaluated. It is revealed that the porosity in the AM produced scaffold is approximately 12% lower than the designed value. There are approximately 68.1 ± 8.6% added materials in the AM produced scaffolds and the added materials are mostly distributed in the places opposite to the building orientation. The building orientation has no effect on the discrepancy in the scaffold porosity and no effect on the distribution of the added materials ($p > 0.05$). Regarding the mechanical properties, the compressive moduli of the scaffolds are 24.4% (produced along the height direction) and 14.6% (produced along the width direction) lower than the designed value and are 49.1% and 43.6% lower than the μFE counterparts, indicating that the imperfect bonding and the partially melted powders have a large contribution to the discrepancy in the compressive modulus of the scaffolds. Compared to the values in the theoretically designed scaffold, the strain energy densities have shifted towards the higher values in the AM produced scaffolds. The findings in the present study provide important information for the design and additive manufacturing of TPMS scaffolds.

Keywords: TPMS scaffold; Additive manufacturing, Geometrical and mechanical properties; Mechanical environment; Finite element analysis

1. Introduction

In the past few years, man-made biomaterials with tailored properties have become the important substitute for human tissues and have been successfully used in many fields, such as the tissue engineering, the sutures and the drug delivery system [**Doulabi et al., 2008; Goncalves et al., 2016; Russo et al., 2013**]. On the other hand, the emerging techniques of additive manufacturing (AM), such as the stereolithography (SLA) and the selective laser melting (SLM), have further driven the design and production of advanced three-dimensional (3D) biomaterials [**Goncalves et al., 2016; Russo et al., 2013; Shirazi et al., 2015**]. Among the various man-made biomaterials, the 3D open cell porous bone scaffold is widely used to replace the damaged bone tissue. For designing bone scaffolds, the triply periodic minimal surface (TPMS) has emerged as an important and widely-used basis, because of the superior features, such as, a mean curvature of zero **[Pinkall and Polthier, 1993]**, a high surface-to-volume ratio **[Yoo, 2014]**. Furthermore, the AM technology has made it feasible to produce bone scaffolds with highly complex microstructures, and consequently the AM technique has been widely used to produce the TPMS-based bone scaffolds **[Atae et al., 2018; Yuan et al., 2019]**. However, it is revealed in previous studies that the imperfections are present in the AM produced scaffolds **[Han et al., 2018; Hussein et al., 2013; Soro et al., 2018; Yan et al., 2017; Zhao et al., 2019]**, which would consequently affect the mechanical and biological performances of the scaffolds, and lead to the early failure of scaffolds **[Campoli et al., 2013]**.

Increasing the precision of the AM technique is one of the approaches to decrease the discrepancy and thus to produce the as-designed product as precise as possible. However, because the quality of the AM products depends on many factors, such as the AM laser power, the powder size, the post-processing and the internal microstructure of the product **[Guan et al., 2013; Hanzl et al., 2015]**, it is very challenging to completely eliminate the errors associated with the AM technique **[Ravari et al., 2014]**. Therefore, the second approach, which is to take into account the scaffold discrepancies in the design stage of scaffold using some advanced statistical methods, is proposed to decrease the discrepancies **[Campoli et al., 2013; Ravari et al., 2014]**. The latter approach is based on the fact that the degree of discrepancies is highly correlated with the geometry of the scaffold **[Yang et al., 2020]**. Therefore, if a large amount of data can be analyzed, the relationship/function between the product discrepancy and the contributing factors can be established and consequently the discrepancy can be largely reduced by introducing these functions into the design stage

[Gorguluarslan et al., 2017; Ravari et al., 2014]. In the attempt to do this, previous studies have quantified the imperfections of the AM produced scaffolds and consequently the defect-coupled model has been proposed **[Huang et al., 2018; Soro et al., 2018]**. However, most of the previous studies have focused on the regular lattice structures **[Huang et al., 2018]**, the microstructure of which can be well described using the dimensional parameters. Quantifying the discrepancy in the TPMS scaffolds is far more challenging than quantifying that in the regular lattice structures, because of the presence of the curved surfaces in the TPMS structures, which have to be described using the mathematical equations. To the authors' knowledge, a systematical quantification of the discrepancy in the TPMS scaffolds is still missing, and especially the discrepancies in the three-dimensional geometry of the scaffold and in the mechanical environment of the scaffold remain unclear.

Additionally, the underlying mechanism explaining the scaffold discrepancy remains unclear and needs to be revealed. For example, regarding the discrepancy in the mechanical properties of the scaffold, one contributing factor is the discrepancy in the scaffold geometry and another one is the status of the powders, such as the bonding status between powders **[Shirazi et al., 2015]**. However, it remains unclear the relative contributions of each influencing factor. Furthermore, when producing the scaffold using the SLM technique, different building orientations can be selected. It has been reported that the AM building orientation has an influence on the various properties of the scaffold **[Soro et al., 2018; Vilaro et al., 2012; Wauthle et al., 2015]**, but it remains unclear whether the building orientation plays a role in the discrepancies in the geometric and mechanical properties of the scaffold, especially in the discrepancies in the 3D geometry of the scaffold and in the mechanical environment of the scaffold.

Therefore, the aims of the present study were to investigate the discrepancies in the geometric and mechanical properties of the theoretically designed and the additively manufactured triply periodic minimal surface-based bone scaffolds and to reveal the underlying mechanism, e.g., the effect of AM building orientation on the discrepancy.

2. Materials and Methods

2.1 Design and additive manufacturing of the TPMS scaffold

The TPMS scaffold with the Gyroid microstructure was designed using K3DSurf (**K3DSurf v0.6.2, Canada**). The dimension of the scaffold was $21.0\times15.0\times15.0$ mm^3, the porosity was 76% and each scaffold consisted of 7×5×5 unit cells. The mathematical equation for the Gyroid surfaces is given as below:

$$U_G = \cos(x)\sin(y) + \cos(y)\sin(z) + \cos(z)\sin(x) - t \quad (1)$$

where, x、y and z are the coordinates of a point in the design space, t is the constant which is used to control the scaffold porosity and it was set to 0.8 in the present study (corresponding to the porosity of 76%). In the present study, the region with $U_G > 0$ was defined as the scaffold and the region with $U_G \leq 0$ was defined as the void.

The designed bone scaffold was manufactured using the SLM technique, which is one of the widely-used AM techniques (**Reinishaw, Wotton-under-Edge, UK**). The Ti-6AL-4V powders with the mean diameter of 19.0 ± 4.3 µm were used to manufacture the bone scaffolds. To investigate whether the AM building orientation had an influence on the properties of TPMS scaffolds, 24 scaffolds were produced along the height (21.0 mm) and the width (15.0 mm) directions of the scaffold (**Figure 1a**) (i.e., 12 scaffolds produced in each direction) using the same AM setting, i.e., the scan speed of 0.04 m/s, the laser power of 350.0 W and the hatch angle of 90 degrees.

2.2 Quantification of the discrepancy in the geometric properties of TPMS scaffold

The discrepancies in the geometric properties of the Gyroid scaffold, including the porosity, the dimension (height and width) and the 3D surface distance, were quantified in the present study (**Figure 1**). On one hand, the values for these parameters were calculated from the theoretically designed scaffolds (**Figure 1a**). On the other hand, the values for these parameters were calculated from the AM produced scaffolds (**Figure 1b**). To do this, the scaffolds were scanned using the µCT scanner (**SkyScan desktop 1172, Bruker, Belgium**) using an image resolution of 31.0×31.0×31.0 µm^3, a voltage of 50.0 kV, a tube current of 200.0 µA and an exposure time of 1180.0 ms. The µCT images were first segmented and the islands were removed in the segmented images (**Figure 1c**). Then the porosity of the scaffold was calculated as the value using the number of scaffold voxels divided by the total number of voxels, and the scaffold height and width were calculated as the averaged distances from one side of the scaffold to the other side. The discrepancy in the 3D surface distance of the scaffold was quantified by superimposing the unit cell model of the theoretically designed scaffold with that of the AM produced one (**Figure 1d – 1f**). In total, 12 unit cell models were extracted from the binary µCT images and then superimposed into the designed unit cell model of the scaffold using the rigid registration algorithm available in the image processing software - Amira (**v5.4.3. FEI Visualisation Sciences Group, France**). Then the distances from the exterior surfaces of the theoretically designed scaffold to those of the AM produced ones were quantified using the in-house developed Matlab code (**R2017a, MathWorks, Natick, Massachusetts, US**). To visualize the geometrical discrepancy in the 3D spatial space of the scaffold, the 'Boolean' operation was performed in the superimposed unit cell models and then the added, the missed and the common parts between the theoretically designed and the AM produced scaffolds were quantified.

2.3 Quantification of the discrepancy in the mechanical properties of TPMS scaffold

The discrepancies in the mechanical properties of the Gyroid scaffold, including the effective compressive modulus and the mechanical environment, were quantified in the present study (**Figure 2**). Regarding the effective compressive modulus, the values were calculated from three different sources, i.e., the first one is from the theoretically designed scaffold (**Figure 2a**), the second one is from the AM produced scaffolds (**Figure 2b**) and the third one is from the µCT images of the scaffolds (**Figure 2c**). The effective compressive modulus of the theoretically designed scaffold was calculated using the numerical homogenization method, i.e., the finite element (FE) model of the designed unit cell of the scaffold with the application of the kinematical periodic boundary condition (KPBC) (**Figure 2d**) **[Lu et al., 2019]**. The KPBC was implemented in ABAQUS using the kinematic coupling, the multi-point constraint equations and the Python code. More details on the definition of KPBC in the FE Gyroid model can be found in the authors' previous publication **[Lu et al., 2019]**. The effective compressive modulus of the AM produced scaffold was calculated from the quasi-static mechanical testing of the scaffold (**Figure 2e**), where the reflective markers were placed on the top and bottom sides of the scaffold and all the scaffolds were compressed along the height direction. The displacements of the markers were recorded using the optical tracking technique and were used to calculate the effective compressive modulus of the scaffold so that the displacement error from the material testing system was eliminated. The third effective compressive modulus of the scaffold was calculated from the micro finite element (µFE) models created from the µCT images of the AM produced scaffolds (**Figure 2f**). The µFE models were generated by converting each scaffold voxel into hexahedron (C3D8) in Mimics (**v20.0, Materialise, Belgium**). In the FE unit cell models meshed using the second-order tetrahedron (C3D10) and the µFE models meshed using the full-integration linear hexahedron (C3D8), the homogeneous, isotropic and linear elastic material model was defined for the base material of the scaffold (i.e., Ti-6AL-

4V), i.e., the elastic modulus of 110.0 GPa and the Poisson's ratio of 0.3 were defined [**Niinomi 1998**]. When calculating the effective compressive modulus, the uniaxial loading along the height direction of the scaffold was defined.

By comparing the effective compressive moduli calculated from three different sources, the discrepancies in the mechanical properties of the TPMS scaffold were quantified and the underlying mechanism was revealed. First, the proportion of the discrepancy, induced by the factors such as the powder bonding status, to the overall discrepancy in the mechanical properties of the scaffold was quantified by comparing the values from the mechanical testing with those from the μFE analysis. Second, the proportion of the discrepancy, induced by the difference in the scaffold geometry, to the overall discrepancy in the mechanical properties of the scaffold was quantified by comparing the compressive moduli from the unit cell analysis with those from the μFE analysis. Lastly, the overall discrepancy in the mechanical properties of the TPMS scaffold was quantified by comparing the compressive moduli from the unit cell analysis with those from the mechanical testing.

Regarding the discrepancy in the mechanical environment of the scaffold, the scaffold under the loading scenario of the uniaxial compression was investigated. The strain energy density (SED) was used to characterize the mechanical environment of the scaffold, because the SED is the resultant value of the corresponding stress and strain components and is highly associated with the bone adaptation behaviors **[Levchuk et al., 2014; Lu et al., 2018]**. The mathematical formulation for the SED is given as below:

$$U = \frac{1}{2}(\sigma_x \varepsilon_x + \sigma_y \varepsilon_y + \sigma_z \varepsilon_z + \tau_{xy}\gamma_{xy} + \tau_{yz}\gamma_{yz} + \tau_{zx}\gamma_{zx}) \quad (2)$$

where, U is the SED, $[\sigma_x\ \sigma_y\ \sigma_z\ \tau_{xy}\ \tau_{yz}\ \tau_{zx}]$ and $[\varepsilon_x\ \varepsilon_y\ \varepsilon_z\ \gamma_{xy}\ \gamma_{yz}\ \gamma_{zx}]$ are the six stress and strain components, respectively. The values of the elemental SEDs can be directly fetched from the FE result files.

The SEDs in the theoretically designed scaffolds were calculated from the FE unit cell model of the scaffold (**Figure 2d**) and the SEDs in the AM produced scaffolds were calculated from the corresponding μFE models (**Figure 2f**). When calculating the SED, a uniform strain of 0.1% was applied on one side of the scaffold along the height direction, while the other side was fully fixed, i.e., all the degrees of freedoms were constrained. It should be noted that because the bone adaptation activities only occur at the exterior surfaces of the scaffold, only the elemental SEDs at the exterior surfaces of the scaffold were outputted from the μFE analysis and then processed using an in-house developed Matlab code. All the FE analysis was performed using the FE software of ABAQUS (**v6.14,**

Dassault Systems SIMULIA Ltd., Providence, RI) and a mesh convergence study was performed for each FE analysis to ensure that the results (i.e., the effective compressive modulus and the SED) were not influenced by the mesh density, which resulted in the element size of approximately 0.06 mm in the FE unit cell model and the element size of 31.0 μm in the μFE models.

2.4 Statistical analysis

The normality for the data within one group was checked using the Shapiro-Wilk test and further confirmed by the visual inspection. When the data were normally distributed, the experimental data were presented as the mean ± standard deviation (SD), and the independent t-test was used to detect the significant difference between groups. When the data were non-normally distributed, the 5th, the median and the 95th percentiles of the data were presented and the Mann-Whitney U test was used to detect the significant difference between groups. The statistical analysis was performed using the PASW statistics 18.0 (SPSS Inc., Chicago, IL) and the probability of type I error was set to 0.05 ($\alpha = 0.05$), i.e., $p < 0.05$ was considered statistically significant.

3. Results

3.1 Discrepancy in the geometric properties of TPMS scaffold

The discrepancies in the porosity, the height and the width of the scaffolds between the theoretically designed and the AM produced groups are significantly different (all $p < 0.05$) (**Figure 3**). When the scaffolds are produced along the height and the width directions, the porosities of the AM produced scaffolds are 9.7% and 10.2% lower than the designed value (76%), respectively (i.e., 68.65 ± 0.64% vs. 76%, and 68.22 ± 1.13% vs. 76%). Regarding the discrepancy in the dimension (height and width), when the scaffolds are produced along the height direction, the width is 3.3% longer than the designed value, i.e., 15.50 ± 0.08 mm vs. 15.00 mm, and the height is 3.0% shorter than the designed value, i.e., 20.37 ± 0.04 mm vs. 21.00 mm. When the scaffolds are produced along the width direction, the width is 4.1% shorter than the designed value, i.e., 14.39 ± 0.05 mm vs. 15.00 mm, and the height is 2.1% longer than the designed value, i.e., 21.44 ± 0.09 mm vs. 21.00 mm. There is no significant effect of the building orientation on the porosity of the AM produced scaffolds ($p = 0.12$). However, the height and the width of the scaffolds produced along the height and width directions are significantly different (both $p < 0.05$) (**Figure 3**).

The deviations (distances) from the exterior surfaces of the AM produced scaffolds to those of the theoretically designed scaffold are not normally distributed. Therefore, the 5th, the median, and the 95th percentiles of the data are reported (**Figure 4**). The 5th, the median, and the 95th percentiles of the surface deviations from the AM produced scaffolds to the theoretically designed scaffold are -0.089 mm, 0.195 mm and 0.552 mm for the scaffolds produced along the height direction and those are -0.095 mm, 0.181 mm and 0.464 mm for the scaffolds produced along the width direction (**Figure 4**). The surface deviations in the scaffolds produced along the height direction are significantly bigger than those in the scaffolds produced along the width direction ($p < 0.05$) (**Figure 4**).

The common parts between the theoretically designed and the AM produced scaffolds are 91.2 ± 5.0%, the missed parts are 9.8 ± 4.9% and the added parts are 68.1 ± 8.6% (taking the volume in the theoretically designed scaffold as the reference). To visualize the distribution of the added materials in the 3D spatial space of the scaffold, the distribution of the probability of the occurrence of the added materials is plotted in **Figure 5**, where the dark grey region represents the theoretically designed scaffold, the 100% region represents the places where the added materials occurred in all the AM produced scaffolds and the 10% region represents the places where the added materials only occurred in 10% of all the AM produced scaffolds, etc. Additionally, it is shown in **Figure 5** that the further the distance from the surfaces of the AM produced scaffold to the surfaces of the theoretically designed scaffold, the lower the probability of the occurrence of the added materials. Furthermore, the added materials are mostly distributed in the places opposite to the building orientation.

3.2 Discrepancy in the mechanical properties of TPMS scaffold

Regarding the discrepancy in the effective compressive modulus, when the scaffolds are produced along the height and the width directions, the compressive moduli of the AM produced scaffolds are 3269.9 ± 90.5 MPa and 3691.1 ± 171.9 MPa, respectively, which are 24.4% and 14.6% lower than the designed value (4323.3 MPa) respectively (taking the designed value as the reference) (both $p < 0.05$) (**Figure 6**). The compressive modulus is significantly higher in the scaffolds produced along the width direction than those produced along the height direction ($p < 0.05$). The representative stress-strain curves from the mechanical testing are shown in **Figure 7**, which shows that slightly different mechanisms are present when the scaffolds are compressed along the height and width directions. When the discrepancy in the scaffold geometry is eliminated, i.e., comparing the results between the AM produced scaffolds and the corresponding μFE models, the compressive moduli of the

AM produced scaffolds are 49.1% and 43.6% lower than the μFE counterparts (taking the μFE value as the reference), i.e., 3269.9 ± 90.5 MPa vs. 6429.2 ± 282.2 MPa when the scaffolds are produced along the height direction, and 3691.1 ± 171.9 MPa vs. 6539.3 ± 298.8 MPa when the scaffolds are produced along the width direction (both $p < 0.05$) (**Figure 6**). The compressive moduli in the two μFE groups are not significantly different from each other ($p = 0.45$). The compressive moduli calculated from the μFE models are 48.7% (scaffolds produced along the height direction) and 51.3% (scaffolds produced along the width direction) higher than the designed value (taking the designed value as the reference) (both $p < 0.05$) (**Figure 6**), implying that some added materials are present in the AM produced scaffolds.

The average SEDs are 1.21 ± 0.20 mJ/m^3 and 1.15 ± 0.07 mJ/m^3 in the scaffolds produced along the height and the width directions, respectively, which are slightly higher than the value (1.14 mJ/m^3) in the theoretically designed scaffolds. To visualize the distribution of the SEDs, the SEDs are divided into five sub-regions and the percentages of the SEDs within each sub-region are counted and plotted in **Figure 8**, which shows that the SEDs have shifted towards the higher values in the AM produced scaffolds, e.g., 71.6 ± 4.24% (scaffolds produced along the height direction) and 72.0 ± 1.18% (scaffolds produced along the width direction) vs. 74.2% (the designed value) for the SEDs between 0.0 mJ/m^3 and 1.0 mJ/m^3, and 2.07 ± 0.23% and 2.11 ± 0.14% vs. 1.6% for the SEDs between 4.0 mJ/m^3 and 5.0 mJ/m^3. The SEDs in the scaffolds produced along the height and the width directions are not significantly different from each other, e.g., 13.2 ± 1.78% vs. 13.3 ± 0.34% for the SEDs between 1.0 mJ/m^3 and 2.0 mJ/m^3 ($p = 0.55$) (**Figure 8**).

4. Discussion

In the present study, the discrepancies in the geometrical and mechanical properties of the theoretically designed and the additively manufactured triply periodic minimal surface (TPMS) scaffolds were investigated.

Compared to the studies in the literature, several novel techniques were used in the present study. First, an image superimposition method was used to visualize and quantify the discrepancies in the 3D spatial space of the scaffold. Second, the μFE models generated from the AM produced scaffolds were analyzed to investigate the influence of the factors, such as the powder bonding, on the discrepancy in the mechanical properties of the scaffold. Therefore, the contributing factors such as the discrepancy in the scaffold geometry are decoupled from other factors. Third, the FE modeling technique was used to calculate the mechanical environment in the theoretically designed and the AM produced scaffolds so that for the first time the discrepancy in the mechanical environment of the scaffold was quantified. Using these novel analysis techniques, several interesting yet important findings are revealed in the present study.

First, it is revealed from the 'Boolean' operation between the theoretically designed and the AM produced scaffolds (after superimposition) that the selective laser melting (SLM) technique produced more materials in the scaffolds. The proportion of the added material to the total material is approximately 68.1%, while the proportion of the missed material to the total material is only 9.8%. Additionally, the data (in the present study) on the distribution of the distances between the theoretically designed and the AM produced scaffolds revealed that the added materials were mostly distributed in the places opposite to the building orientation. Previous studies also revealed that the porosity of the scaffolds produced by SLM is lower than the designed value **[Huang et al., 2018; Soro et al., 2018]**. The reasons for the relatively large proportion of added materials in the produced scaffolds could be that the SLM technique relies on the powders to support the produced structure and thus more powders may be melted at the exterior surfaces of the scaffold **[Huang et al., 2018; Soro et al., 2018]**, especially at the hanging sites. On the other hand, the large surface-to-volume ratio of the TPMS structure (Gyroid) could be the reason that more added materials are produced in the TPMS structure than those in the regular lattice structure (e.g., cubic) **[Yang et al., 2018]**. Regarding the effect of building orientation on the distribution of the added materials, it was revealed that there is no significant difference in the scaffolds produced along the height and width directions, the reason of which could be that the Gyroid scaffold possesses the property of the cubic symmetry **[Lu et al., 2019]**.

Second, it is revealed that the compressive modulus of the AM produced scaffolds is approximately 19.5% lower than the designed value, although more materials are produced in the AM produced scaffolds (The porosities are 76% and 68.4% ± 0.8% in the theoretically designed and the AM produced scaffolds, respectively). When the discrepancy in the scaffold geometry is eliminated, the compressive modulus of the AM produced scaffolds is even lower (46.4%) than the value calculated from the numerical (μFE) counterpart. It should be noted that the μFE model of the scaffold is an ideal representation of the scaffold. While in the present study, the measurement errors in the mechanical testing are well controlled by using the technique such as the optical tracking to record the displacement, it is believed that the discrepancy in the compressive modulus of the scaffolds obtained from the mechanical testing and the μFE analysis is mainly due to reason that the powders are not fully bonded in the AM produced scaffolds, especially at the scaffold exterior surfaces where some un-melted or partially melted powders are present **[Gong et al., 2014; Lewandowski and Seifi, 2016; Rao et al., 2016]**. To confirm this scenario, the scaffolds were imaged using the scanning electron microscope (SEM) with the magnifications of 250 times (**Figure 9a**) and 1250 times (**Figure 9b**). Indeed, some partially melted powders were found at the scaffold surfaces (**Figure 9**). It should be noted that the imperfect bonding and partially melted powders may alter the homogeneity property of the scaffold, which in turn could induce the discrepancies in the mechanical properties of the scaffold, such as the mechanical environment. Regarding the effect of building orientation on the compressive modulus of the scaffold, the compressive modulus in the scaffolds produced along the width direction is significantly higher than those produced along the height direction, which agrees well with the literature data **[Ataee et al., 2018; Hanzl et al., 2015; Vilaro et al., 2012; Yadollahi et al., 2017]**. Vilaro et al. (**2012**) reported that because of the growth of the columnar grain, a strong anisotropy as a function of the building orientation is present in the samples produced by SLM. Guan et al. (**2013**) reported that the tensile properties of the SLM produced samples are the highest at the building orientation of 90 degrees because the direction of the load is perpendicular to the columnar grains. Therefore, when designing and additively manufacturing the TPMS scaffolds, the effect of building orientation on the mechanical properties of the scaffold should be taken into account in the future.

Third, it is revealed that the mechanical environment (strain energy density) in the AM produced scaffolds is different from that in the theoretically designed scaffolds. Compared to the values in the theoretically designed scaffolds, the strain energy densities are shifted towards the higher values, the reason of which could be the discrepancy in the scaffold porosity. It should be noted that the mechanical environment in the AM produced scaffolds is calculated from the μFE analysis, and not from the experimental measurement. It has been shown in the present study that because of the issues related to the imperfect bonding and partially melted powders, the effective compressive moduli of the scaffold obtained from the mechanical testing and the μFE analysis are significantly different from each other. Therefore, the mechanical environment calculated from the μFE analysis may also be affected by the imperfect bonding and the partially melted powders. Nevertheless, there is still no feasible experimental technique available to measure and quantify the mechanical environment (strain energy density) in the AM produced scaffolds.

Some limitations related to the present study should be discussed. First, only one type of the TPMS scaffold is investigated. There are many other types of TPMS scaffolds, such as the Diamond, the Fischer-Koch S, the Double Diamond, etc. **[Blanquer et al., 2017]** and the AM discrepancies in different scaffolds may be different. However, one of the main aims in the present study is to demonstrate the novel approach for quantifying the discrepancy in the geometric and mechanical properties of the TPMS scaffold, e.g., the application of the image superimposition to quantify the geometric discrepancy in the 3D spatial space of the scaffold. Additionally, the method developed in the present study can be easily transferred to analyze other types of scaffolds. Second, only the discrepancies in the geometric and mechanical properties of the TPMS scaffold are investigated. Some other properties of the scaffold, such as the permeability and the cell behavior, are not investigated. It should be noted that both the scaffold permeability and the cell behavior can be influenced by the scaffold geometry **[Callens et al., 2020; Castro et al., 2019]**. Therefore, the discrepancy in the scaffold geometry will induce the discrepancies in the scaffold permeability and the cell behavior, but the extent of the influence still needs further investigations in the future. Third, only the effective compressive modulus of the scaffold under the uniaxial quasi-static loading is investigated in the present study. Some other mechanical properties of the scaffold, such as the fatigue life, the poroviscoelastic behavior, are also crucial when designing scaffolds and the discrepancies in these properties should be addressed in the future studies. Fourth, the mechanical property for the base material of the scaffold (i.e., Ti-6AL-4V) is simplified as homogeneous and isotropic and the FE results presented in the present study should only be interpreted within this context. Previous studies showed that the mechanical property of Ti-6AL-4V is nonhomogeneous and anisotropic **[Hayes et al. 2017; Szafranska et al., 2019]**. Therefore, the multiscale FE model of the scaffold needs to be developed and the research questions investigated in the present study, such as the discrepancy caused by the imperfect bonding of the Ti-6AL-4V powers, have to be revisited in the future. Last but not the least, only the scaffolds produced using the selective laser melting (SLM) technique are investigated. There are many other AM techniques, such as the electron beam melting, the inkjet 3D printing, etc. **[Shirazi et al., 2015]** and the discrepancy in the scaffold property may depend on the AM technique. However, on one hand, the SLM is the technique with a high manufacturing precision and widely used for producing the TPMS scaffold. On the other hand, the methodology developed in the present study is independent of the AM technique and can be easily applied to investigate the discrepancy in the scaffolds produced using other AM techniques.

In summary, it is revealed in the present study that the selective laser melting technique produced more materials in the scaffolds and the added materials are mostly distributed in the places opposite to the building orientation. The compressive moduli of the additively manufactured scaffolds are lower than the designed values due to the imperfect bonding and partially melted powders. These findings provide important information for additively manufacturing the as-designed 3D scaffold, for example, they can help reduce the discrepancy between the theoretically designed and the AM produced scaffolds.

Conflict of interest statement

The authors declare that they have no conflict of interest.

CRediT authorship contribution statement

Yongtao Lu: Conceptualization, Methodology, Software, Investigation, Writing. **Zhentao Cui:** Methodology, Software, Investigation. **Liangliang Cheng:** Resources, Software. **Jian Li:** Methodology, Resources. **Zhuoyue Yang:** Writing – original draft. **Hanxing Zhu:** Conceptualization, Funding acquisition. **Chengwei Wu:** Funding acquisition, Project administration, Supervision.

Funding information

This work was funded by the National Natural Science Foundation of China (grant numbers 11702057, U1908233, 11772086), National Key R&D Program of China (grant numbers 2018YFA0704103, 2018YFA0704104), the Liaoning Provincial Natural Science Foundation of China (grant number 2019-MS-040), DUT-BSU grant (grant number ICR1903) and the State Key Laboratory of Structural Analysis for Industrial Equipment, Dalian University of Technology (grant number GZ19108).

References

Ataee, A., Li, Y.C., Fraser, D., Song, G.S., Wen, C.E., 2018. Anisotropic Ti-6Al-4V gyroid scaffolds manufactured by electron beam melting (EBM) for bone implant applications. Mater. Des. 137, 345-354. https://doi.org/10.1016/j.matdes.2017.10.040.

Blanquer, S.B.G., Werner, M., Hannula, M., Sharifi, S., Lajoinie, G.P.R., Hyttinen, J., Poot, A.A., Grijpma, D.W., 2017. Surface curvature in triply-periodic minimal surface architecture as a distinct design parameters in preparing advanced tissue engineering scaffolds. Biofabrication. 9 (2), 025001. https://doi.org/10.1088/1758-5090/aa6553.

Callens, S.J.P., Uyttendaele, R.J.C., Apachitei, L.E.F., Zadpoor, A.A., 2020. Substrate curvature as a cue to guide spatiotemporal cell and tissue organization. Biomaterials. 232, 119739. https://doi.org/10.1016/j.biomaterials.2019.119739.

Campoli, G., Borleffs, M.S., Yavari, S.A., Wauthle, R., Weinans, H., Zadpoor, A.A., 2013. Mechanical properties of open-cell metallic biomaterials manufactured using additive manufacturing. Mater. Des. 49, 957-965. https://doi.org/10.1016/j.matdes.2013.01.071.

Castro, A.P.G., Pires, T., Santos, J.E., Gouveia, B.P., Fernandes, P.R., 2019. Permeability versus design in TPMS scaffolds. Materials. 12 (8), 1313. https://doi.org/10.3390/ma12081313.

Doulabi, A.S.H., Mirzadeh, H., Imani, M., Sharifi, S., Atai, M., Mehdipour-Ataei, S., 2008. Synthesis and preparation of biodegradable and visible light crosslinkable unsaturated fumarate-based networks for biomedical applications. Polym Adv Technol. 19 (9), 1199-1208. https://doi.org/10.1002/pat.1112.

Gong, H.J., Rafi, K., Gu, H.F., Starr, T., Stucker, B., 2014. Analysis of defect generation in Ti–6Al–4V parts made using powder bed fusion additive manufacturing processes. Addit. Manuf. 1-4, 87-98. https://doi.org/10.1016/j.addma.2014.08.002.

Goncalves, F.A.M.M., Fonseca, A.C., Domingos, M., Gloria, A., Serra, A.C., Coelho, J.F.J., 2017. The potential of unsaturated polyesters in biomedicine and tissue engineering: Synthesis, structure-properties relationships and additive manufacturing. Prog. Polym. Sci. 68, 1-34. https://doi.org/10.1016/j.progpolymsci.2016.12.008.

Gorguluarslan, R.M., Choi, S.K., Saldana, C.J., 2017. Uncertainty quantification and validation of 3D lattice scaffolds for computer-aided biomedical applications. J. Mech. Behav. Biomed. Mater. 71, 428-440. https://doi.org/10.1016/j.jmbbm.2017.04.011.

Guan, K., Wang, Z.M., Gao, M., Li, X.Y., Zeng, X.Y., 2013. Effects of processing parameters on tensile properties of selective laser melted 304 stainless steel. Mater. Des. 50, 581-586. https://doi.org/10.1016/j.matdes.2013.03.056.

Han, C.J., Li, Y., Wang, Q., Wen, S.F., Wei, Q.S., Yan, C.Z., Hao, L., Liu, J., Shi, Y.S., 2018. Continuous functionally graded porous titanium scaffolds manufactured by selective laser melting for bone implants. J. Mech. Behav. Biomed. Mater. 80, 119-127. https://pubmed.ncbi.nlm.nih.gov/29414467.

Hanzl, P., Zetek, M. Baksa, T. Kroupa, T., 2015. The Influence of Processing Parameters on the Mechanical Properties of SLM Parts. Procedia. Eng. 100, 1405-1413. https://doi.org/10.1016/j.proeng.2015.01.510.

Hayer, B.J., Martin, B.W., Welk, B., Kuhr, S.J., Ales, T.K., Brice, D.A., Ghamarian, I., Baker, A.H., Haden, C.V., Harlow, D.G., Fraser, A.H., Collins, P.C., 2017. Predicting tensile properties of Ti-6Al-4V produced via directed energy deposition. Acta. Mater. 133, 120-133. https://doi.org/10.1016/j.actamat.2017.05.025.

Huang, X.H., Zhang, S., Hu, Q.D., Lang, L.H., Gong, S.L., Nielsen, K.B., 2018. Coupling Effect of Unit Cell Topology and Forming Orientation on the Ti6Al4V Porous Structures Fabricated Using Selective Laser Melting. Adv. Eng. Mater. 21 (2),1800737. https://doi.org/10.1002/adem.201800737.

Hussein, A., Hao. L., Yan, C.Z., Everson, R., Young, P., 2013. Advanced lattice support structures for metal additive manufacturing. J. Mater. Process. Tech. 213 (7), 1019-1026. https://doi.org/10.1016/j.jmatprotec.2013.01.020.

Levchuk, A., Zwahlen, A., Weigt, C., Badilatti, S.D., Muller, R., 2014. Large scale simulations of trabecular bone adaptation to loading and treatment. Clin. Biomech. 29 (4), 355-362. https://doi.org/10.1016/j.clinbiomech.2013.12.019.

Lewandowski, J.J., Seifi, M., 2016. Metal Additive Manufacturing: A Review of Mechanical Properties. Ann. Rev. Mater. Res. 46 (1), 151-186. https://doi.org/10.1146/annurev-matsci-070115-032024.

Lu, Y.T., Zhao, W.Y., Cui, Z.T., Zhu, H.X., Wu, C.W., 2019. The anisotropic elastic behavior of the widely-used triply-periodic minimal surface based scaffolds. J. Mech. Behav. Biomed. Mater. 99, 56-65. https://doi.org/10.1016/j.jmbbm.2019.07.012.

Lu, Y.T., Zhao, W.Y., Li, J.Y., Wu, C.W., 2018. Evaluating the theory of bone mechanoregulation in the physiological loading scenario. J. Mech. Med. Biol. 18 (2), 1850011. https://doi.org/10.1142/S0219519418500112.

Niinomi, M., 1998. Mechanical properties of biomedical titanium alloys. Mater. Sci. Eng. A-Struct. Mater. Prop. 243, 231-236. https://doi.org/10.1016/S0921-5093(97)00806-X.

Pinkall, U., Polthier, K., 1993. Computing discrete minimal surfaces and their conjugates, Exp. Math. 2, 15-36. https://doi.org/10.1080/10586458.1993.10504266.

Rao, H., Giet, S., Yang, K., Wu, X.H., Davies, C.H.J., 2016. The influence of processing parameters on aluminium alloy A357 manufactured by Selective Laser Melting. Mater. Des. 109, 334-346. https://doi.org/10.1016/j.matdes.2016.07.009.

Ravari, M.R.K., Kadkhodaei, M., Badrossamay, M., Rezaei, R., 2014. Numerical investigation on mechanical properties of cellular lattice structures fabricated by fused deposition modeling. Int. J. Mech. Sci. 88, 154-161. https://doi.org/10.1016/j.ijmecsci.2014.08.009.

Russo, T., D'Amora, U., Gloria, A., Tunesi, M., Sandri, M., Rodilossi, S., Albani, D., Forloni, G., Giordano, C., Cigada, A., Tampieri, A., De Santis, R., Ambrosio, L., 2013. Systematic analysis of injectable materials and 3D rapid prototyped magnetic scaffolds: from CNS applications to soft and hard tissue repair/regeneration. Procedia. Engineering. 59, 233-239. https://doi.org/10.1016/j.proeng.2013.05.116.

Shirazi, S.F.S., Gharehkhani, S., Mehrali, M., Yarmand, H., Metselaar, H.S.C., Kadri, N.A., Abu Osman, N.A., 2015. A Permeability versus design for tissue engineering: selective laser sintering and inkjet 3D printing. Sci. Technol. Adv. Mater. 16 (3), 033502. https://doi.org/10.1088/1468-6996/16/3/033502.

Soro, N., Attar, H., Wu, X.H., Dargusch, M.S., 2018. Investigation of the structure and mechanical properties of additively manufactured Ti-6Al-4V biomedical scaffolds designed with a Schwartz primitive unit-cell. Mater. Sci. Eng - A. 745, 195-202. https://doi.org/10.1016/j.msea.2018.12.104.

Szafranska, A., Antolak-Duda, A., Baranowski, P., Bogusz, p., Zasada, D., Malachowski, J., Czujko, T., 2019. Identification of mechanical properties for titanium alloy Ti-6Al-4V produced using LENS technology. Materials. 12 (6), 886. https://doi.org/10.3390/ma12060886.

Vilaro, T., Colin, C., Bartout, J.D., Naze, L., Sennour, M., 2012. Microstructural and mechanical approaches of the selective laser melting process applied to a nickel-base superalloy. Mater. Sci. Eng. A - Struct. Mater. Prop. Microstruct. Process. 534, 446-451. https://doi.org/10.1016/j.msea.2011.11.092.

Wauthle, R., Vrancken, B., Beynaerts, B., Jorissen, K., Schrooten, J., Kruth, J.P., Humbeeck, J.V., 2015. Effects of build orientation and heat treatment on the microstructure and mechanical properties of selective laser melted Ti6AI4V lattice structure. Addit. Manuf. 5, 77-84. https://doi.org/10.1016/j.addma.2014.12.008.

Yadollahi, A., Shamsaei, N., Thompson, S.M., Elwany, A., Bian, L., 2017. Effects of building orientation and heat treatment on fatigue behavior of selective laser melted 17-4 PH stainless steel. Int. J. Fatigue. 94, 218-235. https://doi.org/10.1016/j.ijfatigue.2016.03.014.

Yan, C.Z., Hao, L., Hussein, A., Wei, Q.S., Shi, Y.S., 2017. Microstructural and surface modifications and hydroxyapatite coating of Ti-6Al-4V triply periodic minimal surface lattices fabricated by selective laser melting. Mater. Sci. Eng-C. Mater. Biol. Appl. 75, 1515-1524. https://doi.org/10.1016/j.msec.2017.03.066.

Yang, L., Ferrucci, M., Mertens, R., Dewulf, W., Yan, C.Z., Shi, Y.S., Yang, S.F., 2020. An investigation into the effect of gradients on the manufacturing fidelity of triply periodic minimal surface structures with graded density fabricated by selective laser melting. J. Mater. Pro. Tech. 275, 116367. https://doi.org/10.1016/j.jmatprotec.2019.116367.

Yang, L., Yan, C.Z., Han, C.J., Chen, P., Yang, S.F., Shi, Y.S., 2018. Mechanical response of a triply periodic minimal surface cellular structures manufactured by selective laser melting. Int. J. Mech. Sci. 148, 149-157. https://doi.org/10.1016/j.ijmecsci.2018.08.039.

Yoo, D.J., 2014. Advanced porous scaffold design using multi-void triply periodic minimal surface models with high surface area to volume ratios. Int. J. Precis. Eng. Manuf. 15, 1657-1666. https://doi.org/10.1007/s12541-014-0516-5.

Yuan, L., Ding, S.L., Wen, C.E., 2019. Additive manufacturing technology for porous metal implant applications and triply minimal surface structures: A review. Bioact. Mater. 4 (1), 56-70. https://doi.org/10.1016/j.bioactmat.2018.12.003.

Zhao, L., Pei, X., Jiang, L.J., Hu, C., Sun, J.X., Xing, F., Zhou, C.C., Fan, Y.J., Zhang, X.D., 2019. Bionic design and 3D printing of porous titanium alloy scaffolds for bone tissue repair. Compos. Part. B - Eng. 162, 154-161. https://doi.org/10.1016/j.compositesb.2018.10.094.

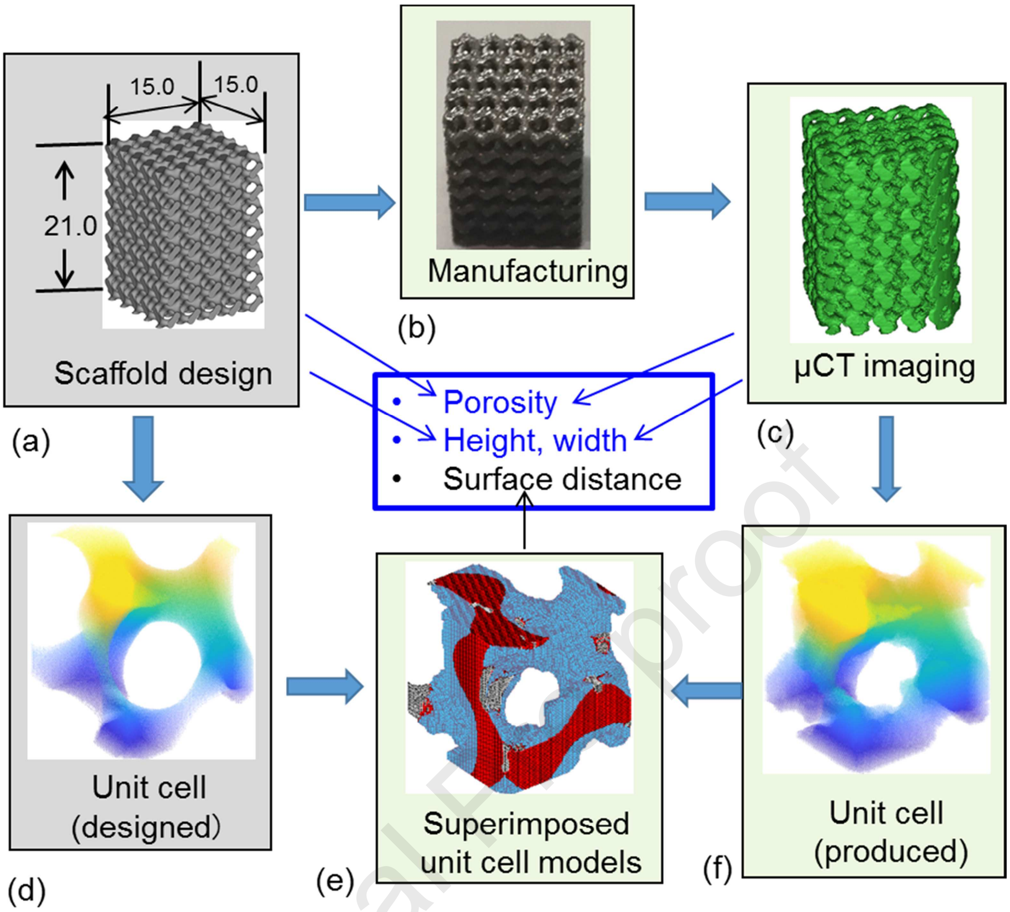

Figure 1: Workflow for quantifying the discrepancy in the geometric properties of the TPMS scaffold

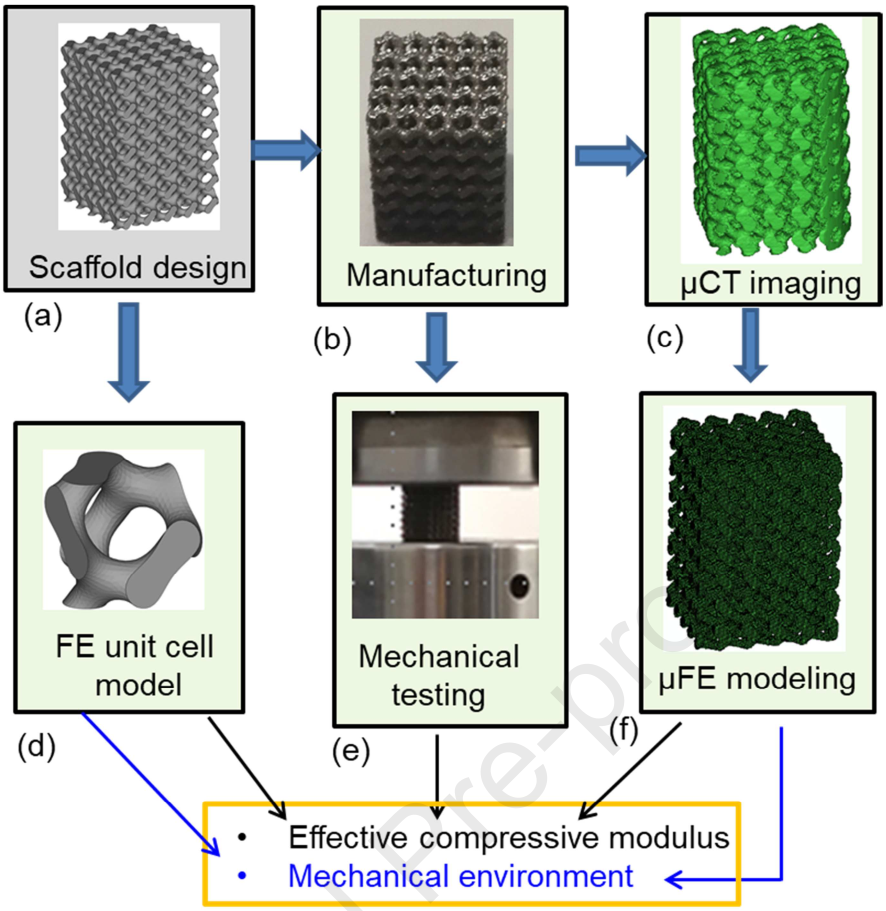

Figure 2: Workflow for quantifying the discrepancy in the mechanical properties of the TPMS scaffold

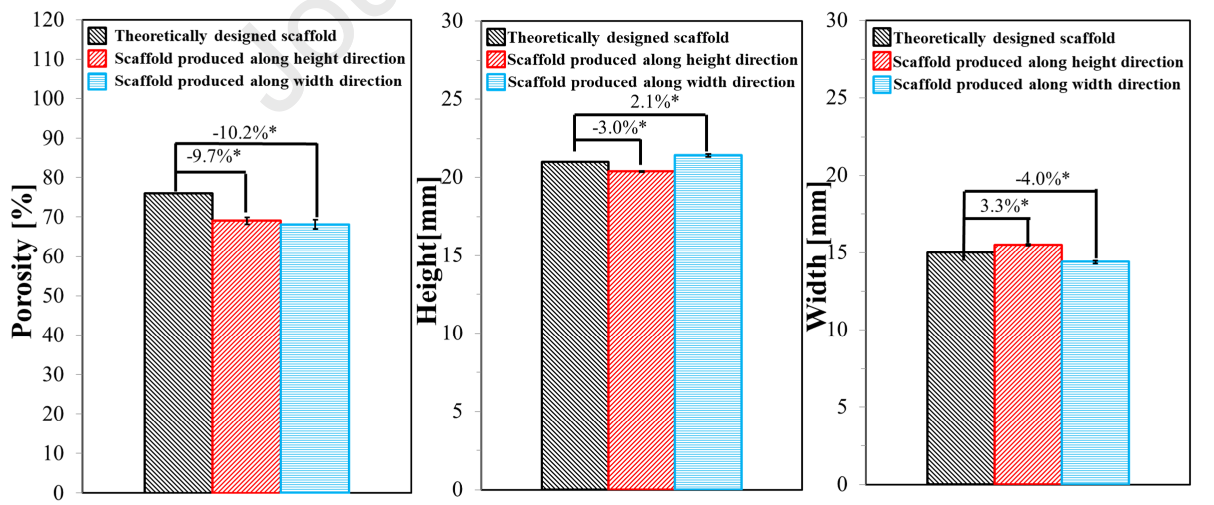

Figure 3: Quantification of the discrepancies in the porosity, the height and width of the scaffold in the theoretically designed and additively manufactured Gyroid scaffolds (* $p<0.05$)

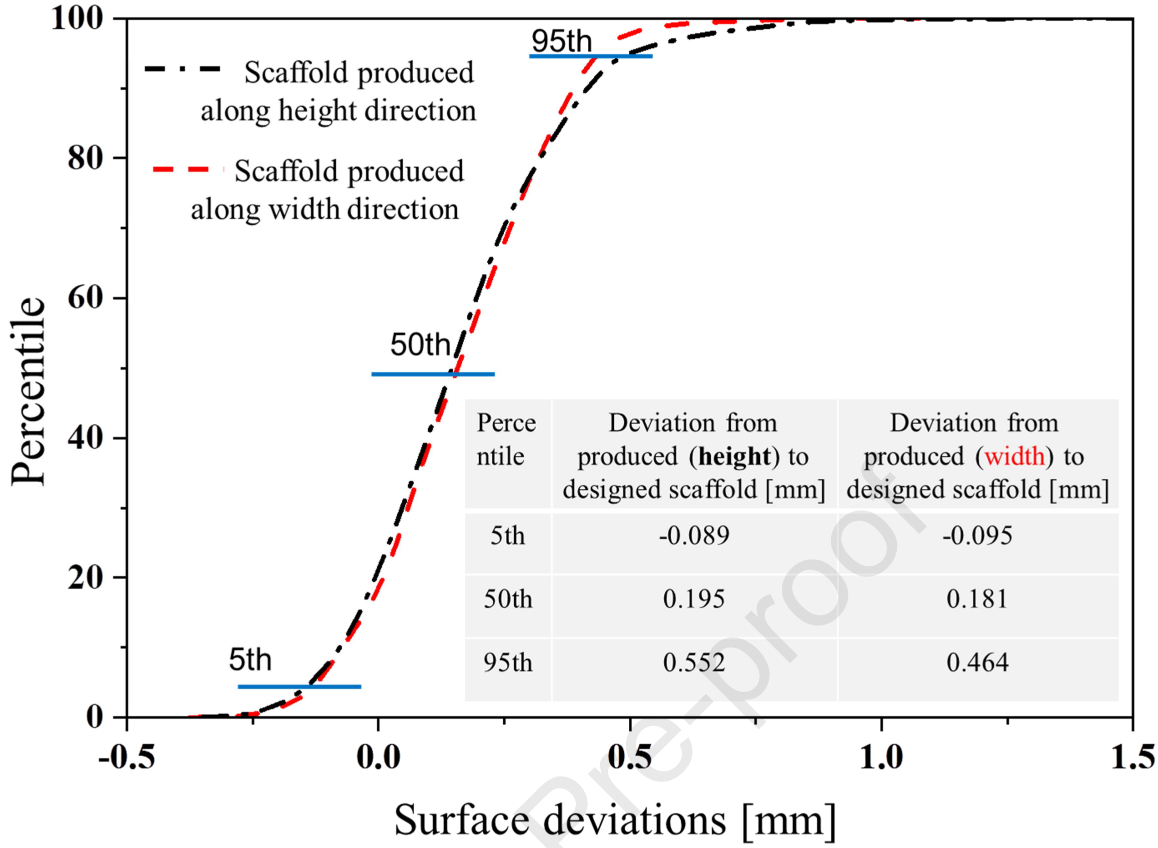

Figure 4: Quantification and distribution of the deviations (distances) from the exterior surfaces of the produced scaffolds to those of the designed scaffold (the positive values represent the surfaces of the AM produced scaffold are in the outside spaces of the designed scaffolds, while the negative values represent the surfaces inside the designed scaffold)

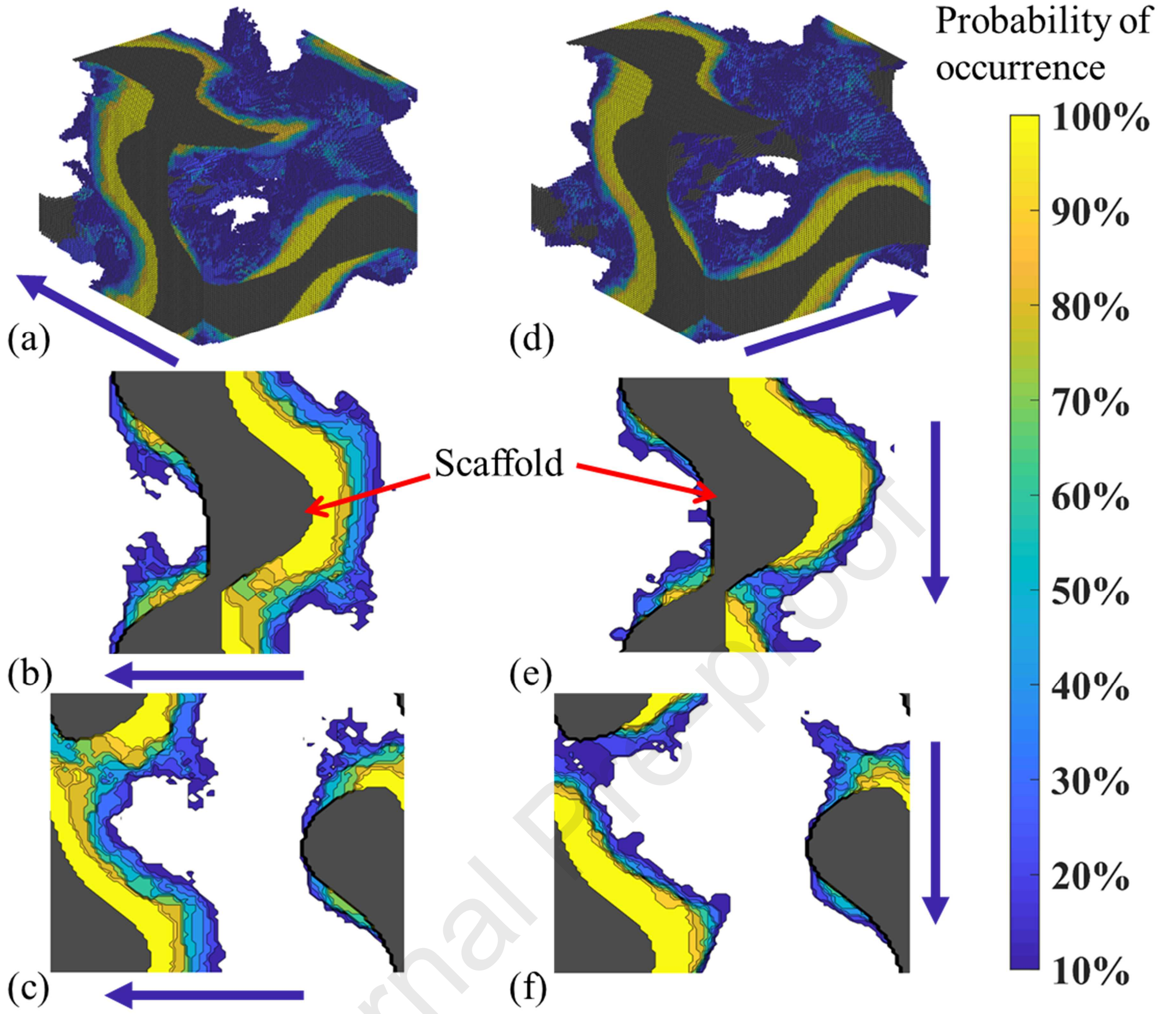

Figure 5: Distribution of the occurrence probability of the added materials in the 3D spatial space of the scaffold (blow arrow represents the building orientation of the additive manufacturing)

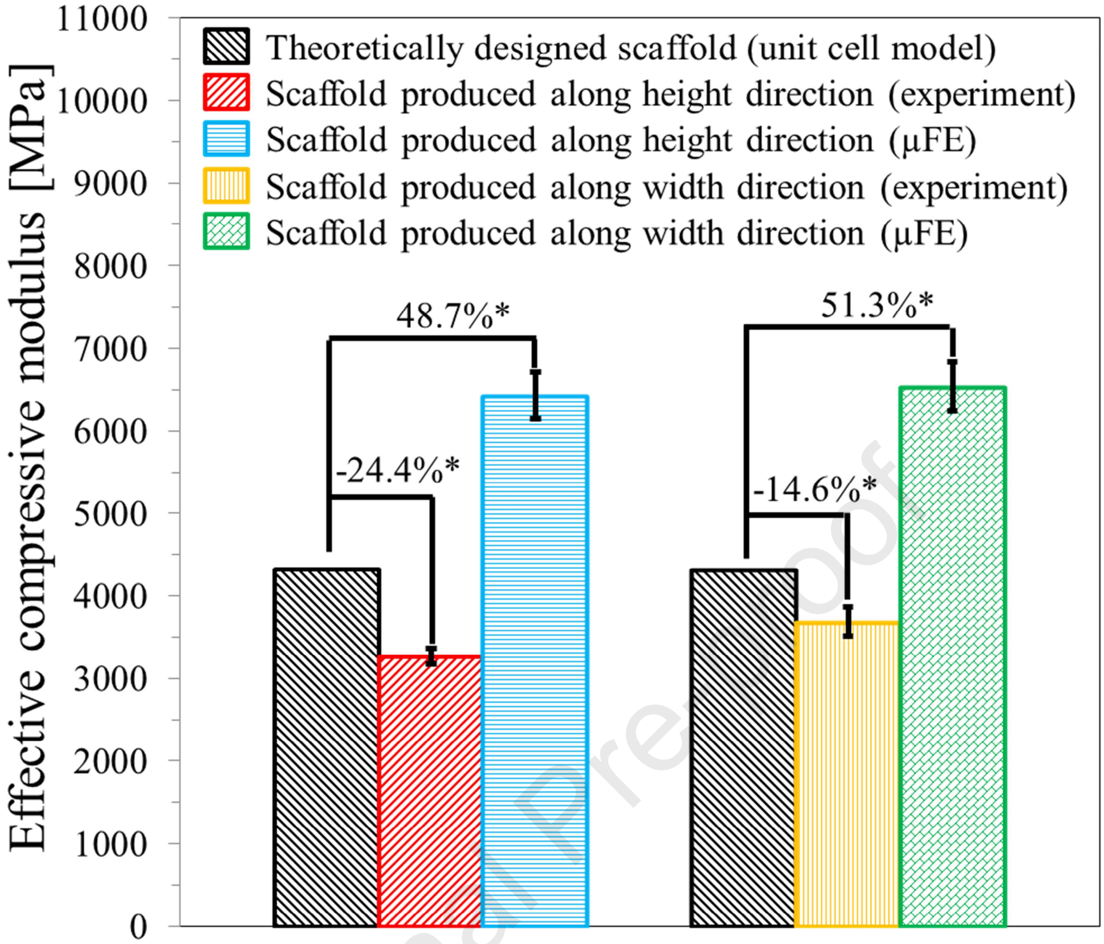

Figure 6: Quantification of the discrepancies in the effective compressive modulus of the scaffolds among the theoretically designed, the mechanical testing and the μFE analysis values (* $p<0.05$)

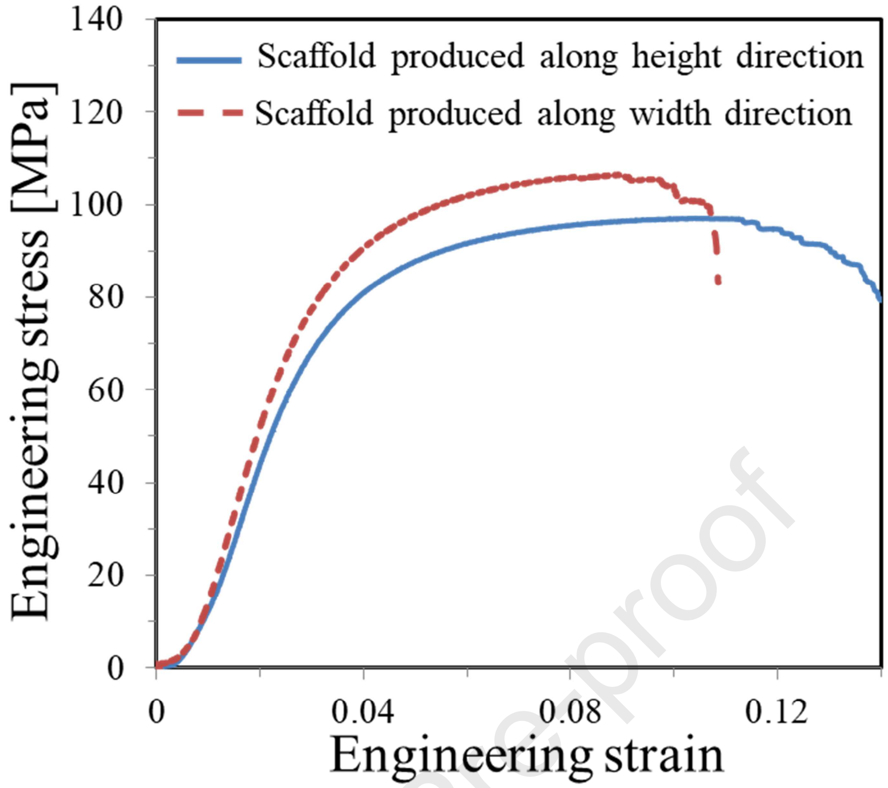

Figure 7: The representative stress strain curves from a scaffold produced along the height direction and a scaffold produced along the width direction. All the mechanical compression tests are performed along the scaffold height direction.

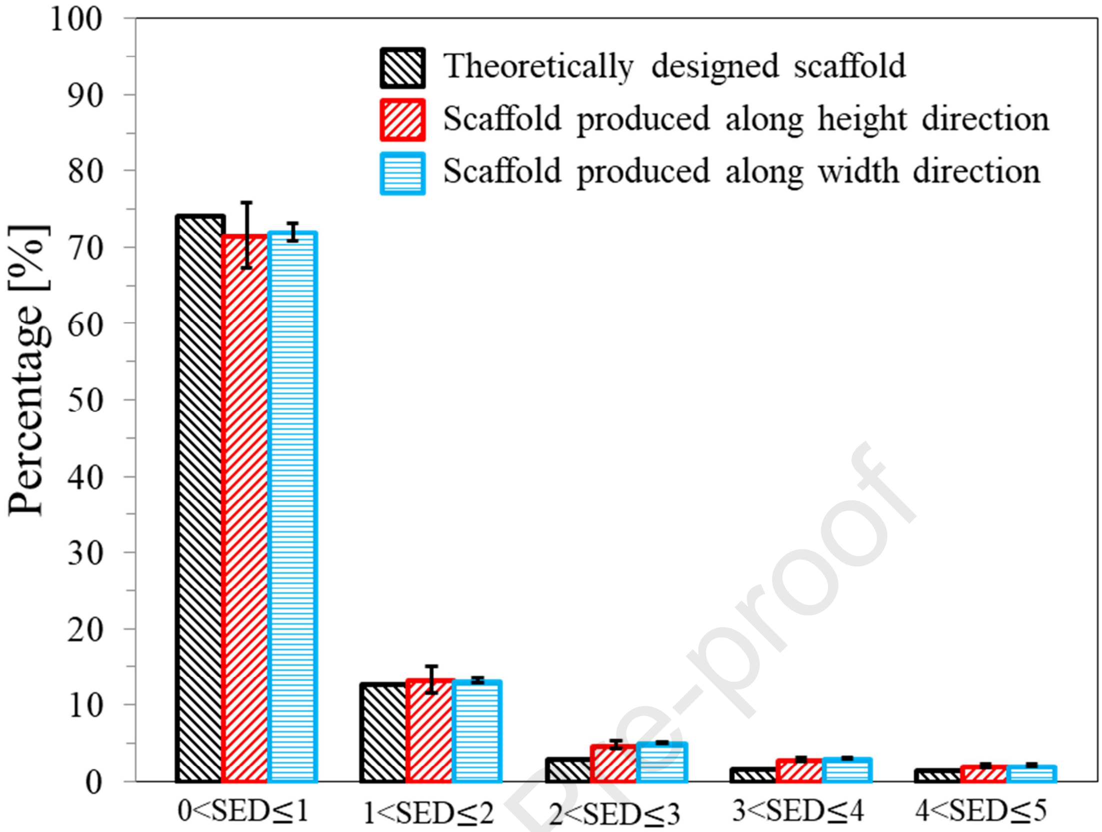

Figure 8: Distribution of the strain energy density (SED) in the theoretically designed and the additively manufactured scaffolds

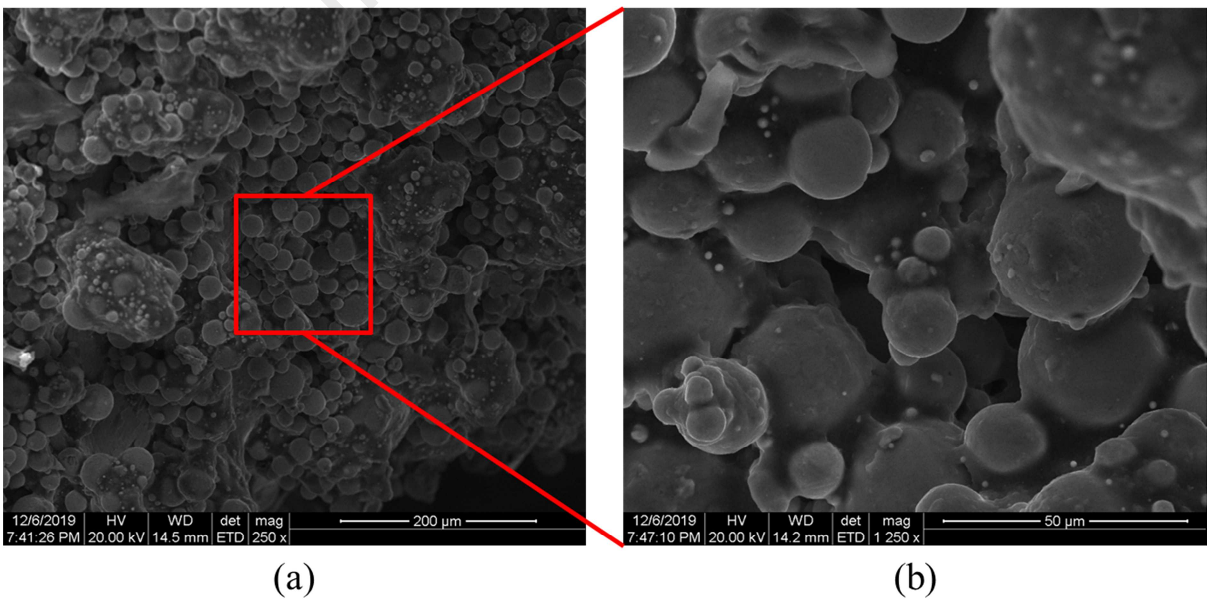

Figure 9: Scanning electron microscope (SEM) images of the scaffold made by the selective laser melting technique, (a) magnification of 250 times and (b) magnification of 1250 times

Declaration of interests

☒ The authors declare that they have no known competing financial interests or personal relationships that could have appeared to influence the work reported in this paper.

☐The authors declare the following financial interests/personal relationships which may be considered as potential competing interests: